Sören Ehlers, Joep Broekhuijsen, Hagbart S. Alsos, Florian Biehl, and Kristjan Tabri. 2008. Simulating the collision response of ship side structures: A failure criteria benchmark study. International Shipbuilding Progress, volume 55, numbers 1-2, pages 127-144.

© 2008 IOS Press

Reprinted with permission from IOS Press.

International Shipbuilding Progress 55 (2008) 127–144
DOI 10.3233/ISP-2008-0042
IOS Press


# Simulating the collision response of ship side structures: A failure criteria benchmark study

Sören Ehlers [a,*], Joep Broekhuijsen [b], Hagbart S. Alsos [c], Florian Biehl [d] and Kristjan Tabri [a]

[a] *Department of Mechanical Engineering, Helsinki University of Technology, Helsinki, Finland*
[b] *Schelde Naval Shipbuilding, Vlissingen, The Netherlands*
[c] *Department of Marine Technology, The Norwegian University of Science and Technology, Trondheim, Norway*
[d] *Technical University of Hamburg, Institute for Ship Structural Design and Analysis, Hamburg, Germany*

Simulations of the collision response of three different ship side structures are performed using the finite element method. The aim is to obtain a force–penetration curve based on the inner mechanics without considering outer dynamics. Respective structures were previously tested in large scale under the right angle ship–ship collision with a bulbous bow and these experiments were used to validate the simulations. The analysis focus is to determine the influence on the collision results from different failure criteria including the mesh size sensitivity. This paper applies the Germanischer Lloyd (GL) criterion based on thru thickness plastic strain, the criterion based on studies of Peschmann and the Rice–Tracey and Crockcroft–Latham (RTCL) criterion. The comparison of results attained here with the experimental results brings an insight into the sensitivity of the failure criteria. The final conclusion of this work is the performance of the studied failure criteria and further guidelines for collision or grounding simulations.

Keywords: FEM, non-linear, LS-DYNA, failure criteria, large scale experiments

## 1. Introduction

Numerical ship collision and grounding simulations are increasingly being performed. Safety at sea in the maritime environment is a crucial issue. Designing novel crashworthy ship structures becomes an important issue in today's research needs. Reliable and realistic simulations of the collision or grounding phenomena are required. These simulations include highly non-linear structural deformations until rupture, specifically failure of certain elements [1,2]. Simulating rupture entails the need for precise material models and failure criterion to address the failing elements. Until the point of necking the material behavior can be captured well with the finite

*Corresponding author: S. Ehlers, Department of Mechanical Engineering, Ship Laboratory, Helsinki University of Technology, Tietotie 1C, 02015 TKK, Helsinki, Finland. Tel.: +358 9 451 3497; Fax: +358 9 451 4173; E-mail: soeren.ehlers@tkk.fi.

0020-868X/08/$17.00 © 2008 – IOS Press and the authors. All rights reserved

element method, but beyond the onset of necking, the correspondence to reality may be very poor.

A blindfold benchmark study using three failure criteria with equal finite element meshes, material data and boundary conditions were performed with LS-DYNA. The failure criteria were the GL based thru thickness strain criterion, a criterion based on Peschmann [3] and the RTCL (Rice–Tracey and Crockcroft–Latham) criterion [4,5].

Since all the applied criteria depend upon the mesh size, a mesh size sensitivity analysis was performed. Furthermore, in order to verify the various material routines involved in the analyses, simulation without failure was performed.

The benchmark study consists of three ship side structures that were experimentally tested for collision in large scale. Validation of the failure criteria was obtained by comparing experimental and numerical force–penetration curves. The experiments and simulations were performed until the rupture of the inner plating occurred. The effect of welding was not considered in this study.

Simulating the experimental boundary conditions was a critical issue, because the clamping system in the experiment was not critically assessed. Hence, a fully rigid clamping system was assumed. For the third test structure a comparison to the real clamping system according to Peschmann [3] was made, resulting in a higher absorbed energy.

## 2. Large scale experiments

During the period of 1997 to 1998 a series of 4 large-scale collision experiments were performed in the Netherlands by TNO (the Dutch institute for applied physical research) on behalf of a Japanese, German, Dutch consortium of shipyards and one classification society. Each test for the individual members had its own purpose, such as the validation of numerical analysis techniques, testing new structural concepts and understanding the various aspects involved in this type of accident. In this benchmark the test data of the experiments was used to test the applicability of different failure criteria. The experiments were conducted under the Association for Structural Improvement of the Shipbuilding Industry (ASIS) [6] and the Hamburg University of Technology [7]. The test facility consisted of a 800 tons inland waterway tanker Nedlloyd 34 striking a 1400 tons inland waterway tanker Amatha at a 90° angle with a speed of around 4 m/s. Based on the argument that collision damage is usually limited to a restricted area of the side structure, depending on the striking bow, the size of the test section was chosen to be: length $\times$ width $= 7.9 \times 4.5$ m. The test section was mounted via a set of clamps through the load measuring devices to a stiffened section in the target vessel Amatha. On the striking ship Nedlloyd 34 a bulbous bow, filled with concrete, was mounted. The supporting structure of the bow was connected via a set of load measuring cells to the striking ship, see Fig. 1. The loads and penetration were recorded during the tests and used for the benchmark. The experiment consisted of the three different test sections; a stiffened plate (see Fig. 2), a sandwich panel (see Fig. 3) and a conventional double hull section (see Fig. 4).

Fig. 1. Experimental set-up.

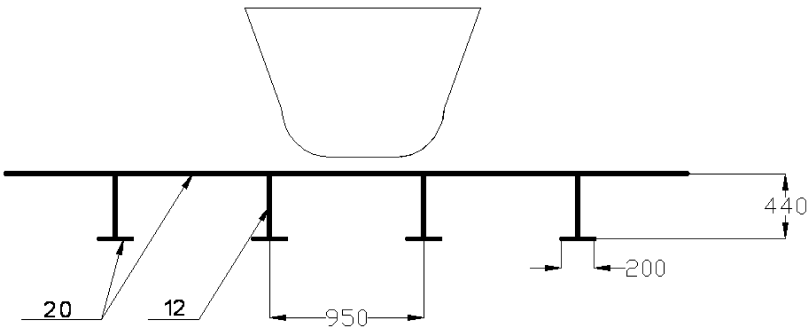


Fig. 2. Test section 1 (dimensions are in mm).

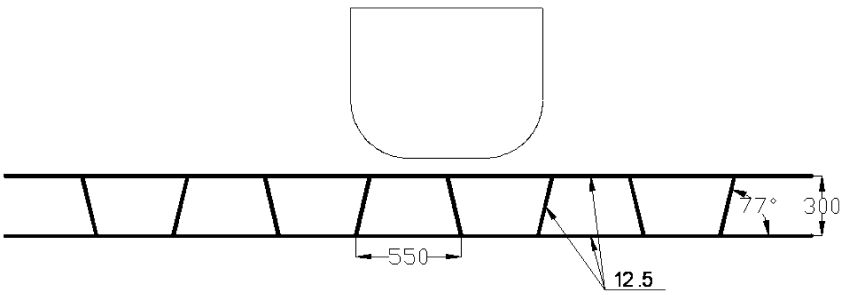


Fig. 3. Test section 2 (dimensions are in mm).

## 3. Numerical modeling

The analyses were performed using the explicit time integration solver LS-DYNA. LS-DYNA can analyze large deformations with dynamic response using finite element methods. The structures were modeled using four noded quadrilateral Belytschko–Lin–Tsay shell elements with 5 integration points through the thickness. This element type is one of the most commonly used elements in the numerical

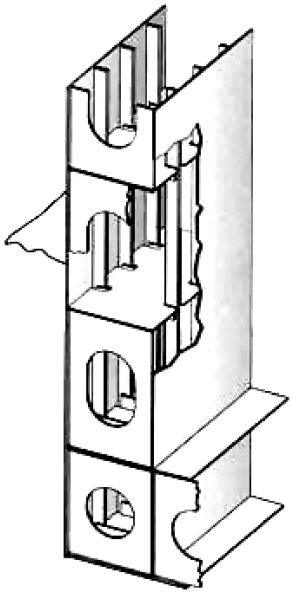

Fig. 4. Test section 3.

analysis of crash mechanics of thin-walled structures, and the default shell element in LS-DYNA. It was demonstrated in numerous examples that these elements capture the plastic collapse of plate structures accurately as long as no cracks are propagating; see for example [8].

Mesh size sensitivity at fracture is another challenge of the simulations, see [4,5] and [9]. Shell elements are highly sensitive to this effect, which is caused by the discrete nature of the mesh. This is due to local effects around the crack or other details that cannot be captured by the mesh itself. Differences in the mesh will therefore yield different critical damage values at fracture. The plane stress definition of shells also complicates this effect when localized necking occurs, due to the lack of stress resistance in the thickness direction. The last effect tends to even out when the shell element becomes much larger than the shell thickness itself. The mesh effect due to local necking can be accounted for with curve fit relations. For example will coarse meshed, 100 mm mesh size in Figs 5–7, yield a different fracture strain than more refined models. As the applied criteria depend upon the mesh size, a mesh size sensitivity analysis is performed analyzing each of the three test structures with a uniform rectangular element size of 25, 50 and 100 mm. For the 50 mm mesh, a simulation is performed without subjected failure criterion to verify the compliance of the results obtained by different material models in LS-DYNA.

The initiation and propagation of fracture in the structure was modeled in LS-DYNA by deleting the failing elements from the model. Differences in fracture propagation arising from the applied criteria were analyzed.

The most general contact treatment was applied through the *CONTACT_ AUTOMATIC_SINGLE_SURFACE contact scheme, where the reaction forces between structure and indenter are obtained by the *CONTAC_FORCE_

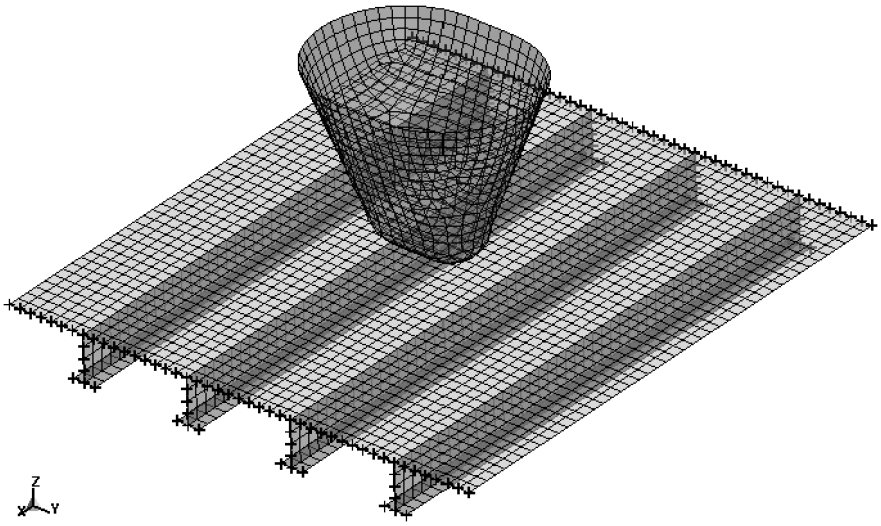


Fig. 5. Test 1 model with 100 × 100 mm element size.

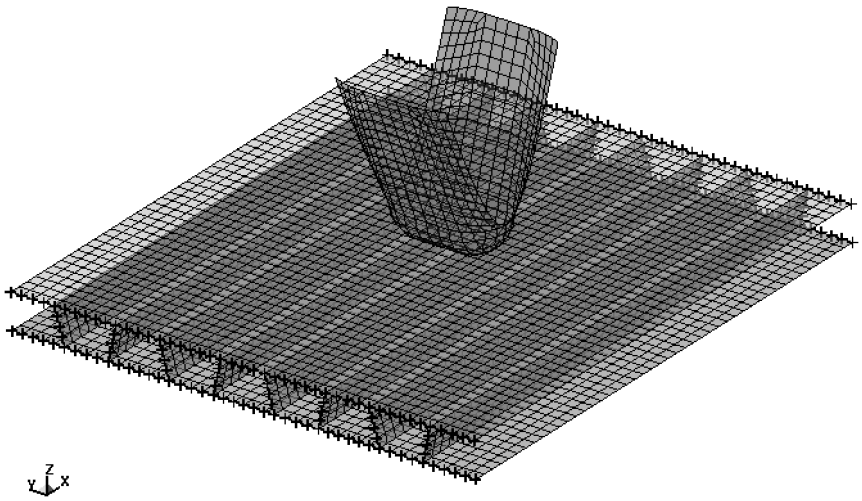


Fig. 6. Test 2 model with 100 × 100 mm element size.

TRANSDUCER_PENALTY card. The *CONTACT_… are LS-DYNA specific input file options, defining how the contact is treated and how the resulting force are computed [10]. The automatic single surface uses nodal normal projections resulting in a continuous contact surface. The force transducer penalty defines the body, respectively the indenter, from which the contact forces are measured. A static friction coefficient of 0.3 was used.

The calculations were displacement controlled. The rigid indenter was moved into the structure with a constant velocity of 10 m/s. Dynamics were neglected and therefore not considered in the analysis. The boundary conditions are in compliance with the experimental set up, and assumed to be fully clamped at the edges parallel to the $y$ axis (indicated by the symbol "+" in Figs 5–7) and free at the remaining edges.

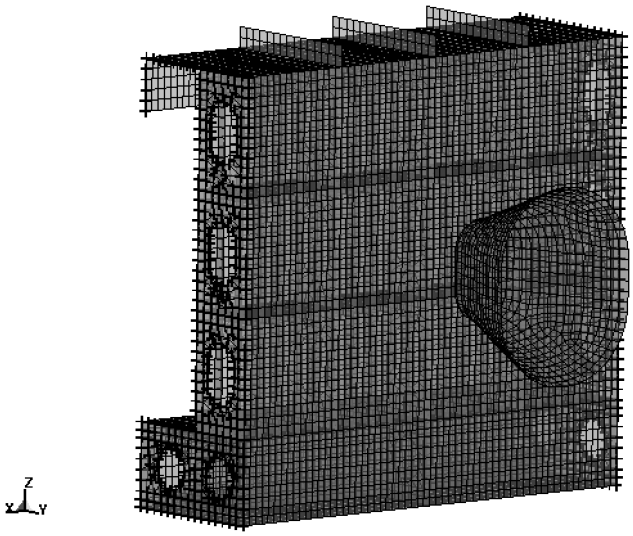


Fig. 7. Test 3 model with 100 × 100 mm element size.

## 4. Material properties

The common engineering tensile test formed the basic material information for the applied failure criteria used in the simulations. The engineering stress–strain curve was constructed from the load elongation measurements. LS-DYNA requires for an input the true stress–strain curve, where the stress and strain becomes non-linear as a function of the true cross-sectional area of the specimen. The true stress–strain curve was obtained as presented by Peschmann [3] and by reverse engineering resulting in the following power law of the form

$$\sigma = K \cdot \mathrm{e}^n \tag{1}$$

with a strength coefficient $K = 730$ and a strain hardening index $n = 0.20$. The experimental yield stress was found to be 284 MPa (see Fig. 8). The Young's Modulus equaled 206 MPa, Poisson ratio equals 0.3 and the steel density was 7850 kg/m$^3$.

## 5. Theoretical background of the thru thickness strain criterion

Thinning strain, or thru thickness strain, in shell elements is evaluated on the basis of the incompressibility condition. This condition can easily be presented for the uniaxial tension [12], which states that

$$\mathrm{d}\varepsilon_2^P = \mathrm{d}\varepsilon_3^P = -\frac{1}{2}\,\mathrm{d}\varepsilon_1^P, \tag{2}$$

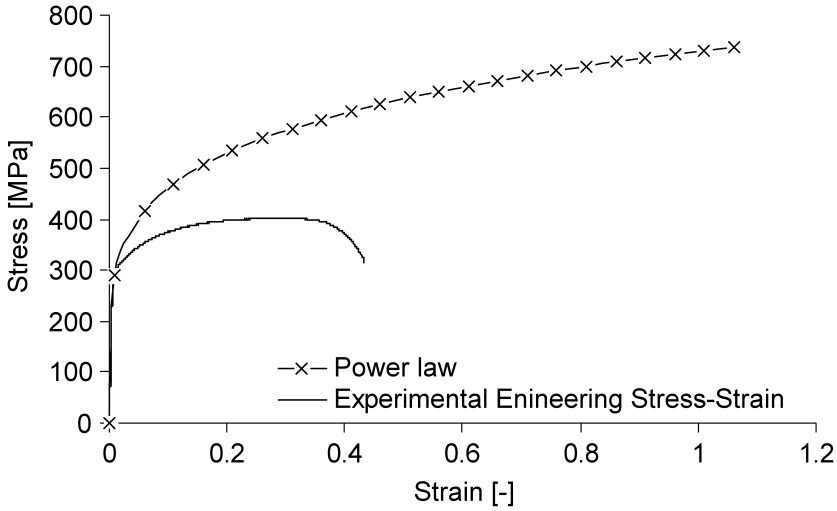


Fig. 8. Stress–strain relations of the simulations material [11].

from which the through thickness failure strain $\mathrm{d}\varepsilon_{3,f}$ criterion can be evaluated as a function of critical strain $\mathrm{d}\varepsilon_{1,f}$ in uniaxial tension as

$$\mathrm{d}\varepsilon_{3,f} = -\frac{1}{2}\,\mathrm{d}\varepsilon_{1,f}. \tag{3}$$

The thru thickness strain criterion in LS-DYNA erases an element if the through thickness strain reaches its critical limit.

### *5.1. Evaluation of equivalent plastic strain and mesh sensitivity according to GL*

To evaluate the critical thru thickness strain at the moment of fracture, an empirical criterion is presented by [13] and [14]:

$$\varepsilon_f(l_e) = \varepsilon_g + \varepsilon_e \cdot \frac{t}{l_e}, \tag{4}$$

where $\varepsilon_g$ is the uniform strain and $\varepsilon_e$ is the necking strain, $t$ is the plate thickness and $l_e$ is the individual element length. It is commonly recommended that the ratio $l_e/t$ is not less than 5 for shell element. The values of uniform and necking strain achieved from thickness measurements related to the calculated stress states given in [13] are 0.056 for the uniform strain and 0.54 for the necking strain in the case of shell elements.

Implementation of those values is performed for material model 123 of LS-DYNA [10]. Material 123 is a modified piecewise linear plasticity model using the stress versus strain curve defined in Fig. 8. This material model allows fractures based on plastic thinning. The pre-calculated critical strain values are input for the material

definition. The critical strain values are a function of the actual shell thickness and the prescribed element size of 25, 50 and 100 mm. The criterion will be referred to as “GLF”.

## 6. Theoretical background of the criterion based on Peschmann

In sheet metal forming the desired shape has to be obtained without tearing. The maximum strains that can be attained in sheet metal forming prior to localized necking are called the forming limit strains. A representation of these limit strains in the principal strain space is generally called a forming limit diagram, see Fig. 9. The region above the forming limit curve represents the strains at which local necking failure occurs and below the forming limit curve the material can be stretched without localized necking. The minimum major strain values occur at or near zero minor strains, under the so-called plain strain condition.

Unfortunately, common criteria for localized necking, derived from the theory of plasticity, only holds true for the thin shells to a maximum of 3 mm. The plate thicknesses of the test sections are significantly thicker. Hence, for plates of this thickness the stress triaxiality in the necking region should be taken into account. Forming limit diagrams have to be obtained experimentally.

### *6.1. Evaluation of equivalent plastic strain and mesh sensitivity according to Peschmann*

Peschmann [15] obtained those forming limit diagrams experimentally from the test section 3 to evaluate the equivalent plastic strain at different locations at the

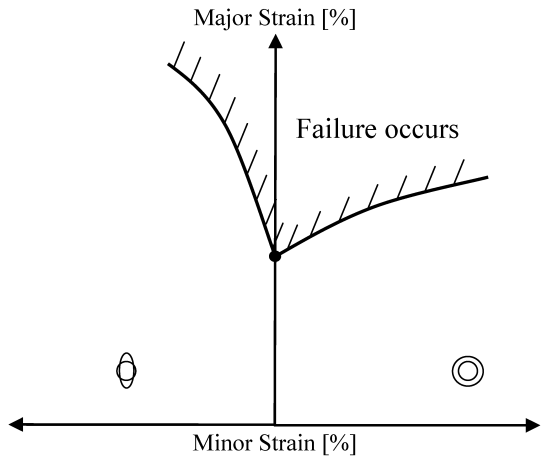


Fig. 9. Principle forming limit diagram.

moment of fracture. With the given relation,

$$\varepsilon_f(l_e) = \varepsilon_g + \alpha \cdot \frac{t}{l_e}, \tag{5}$$

where $\varepsilon_g$ is the uniform strain, $\alpha = \varepsilon_m \cdot (x_e/t)$ is a factor depending on the necking strain and the length of the neck, $t$ is the plate thickness and $l_e$ is the individual element length. Equation (5) is the basis of Eq. (4). It is commonly recommended that the ratio $l_e/t$ is not less than 5 for shell elements. For the plate thicknesses of 5 mm Peschmann obtained $\varepsilon_g = 1$ and $\alpha = 0.8$. For plate thicknesses of 12.5–20 mm Peschmann obtained $\varepsilon_g = 0.08$ and $\alpha = 0.65$. The criterion proposed by Peschmann will be referred to as "PES".

### *6.2. Implementation of the PES criterion*

The element failure routine was implemented in a user defined material model similar to material 24 of LS-DYNA [10]. Material 24 is a piecewise linear isotropic plasticity model utilizing the material behavior defined in Fig. 8. First the geometric values $t$ and $l_e$ were obtained for each individual element. The plate thicknesses can be obtained directly from LS-DYNA. The characteristic element length was calculated from the nodal coordinates. With the given values for $\varepsilon_g$ and $\alpha$, an individual plastic failure strain for each element was obtained. Once the element yielded, plastic failure strain was compared to the effective plastic strain of the element. The stresses in each layer were set to zero once the strain in the integration point exceeds the limit set by the criterion. The element was deleted since all the integration points failed.

## 7. Theoretical background of the RTCL criterion

The RTCL criterion is a combination of two continuum damage models, the Rice–Tracey [16] and Crockcroft–Latham damage model [17]. Together they cover the full stress triaxiality range, defined by the hydrostatic stress

$$\sigma_m = \frac{1}{3}(\sigma_1 + \sigma_2 + \sigma_3) \tag{6}$$

over the effective stress $\sigma_e$, yielding the following expression

$$T = \frac{\sigma_m}{\sigma_e}. \tag{7}$$

Compared to the effective strain criterion which in the "effective strain–stress triaxiality" plane shows a constant ductility for all stress states, the RTCL model will

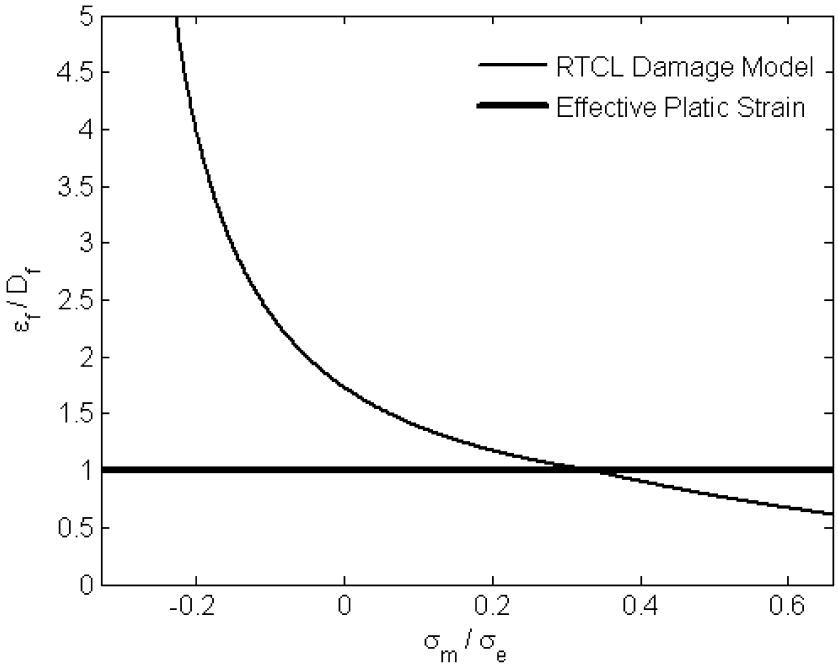


Fig. 10. The failure criterion over the stress triaxiality range.

yield a very ductile material response in compression and shear states. As the stress triaxiality increases, the material will respond more brittle-like, Fig. 10. For shell elements this maximum comes at a triaxiality equal to $T = 2/3$, which is seen as biaxial tensional loading.

The RTCL criterion is presented and verified by Törnqvist at DTU [4] and [5], although, Rice–Tracey and Cockcroft–Latham criteria dates back to the late sixties. The RTCL expression yields

$$D = \int \frac{\sigma_1}{\sigma_e} \, \mathrm{d}\varepsilon_e \qquad \text{if } -0.33 < T < 0.33, \tag{8}$$

$$D = \int \frac{1}{C} \exp\left(\frac{3\sigma_m}{3\sigma_e}\right) \mathrm{d}\varepsilon_e \quad \text{if } T > 0.33, \tag{9}$$

where $D$ is the damage variable, $\sigma_1$ is the major principal stress, and $\mathrm{d}\varepsilon_e$ is the effective plastic strain increment. Figure 10 shows the comparison between the RTCL model given by the thick line and the constant effective plastic strain model shown by the stapled line. The two models will intersect at $T = 0.33$ if $C = 1.65$, that is at uniaxial tension, which means that the RTCL model can be calibrated by a single tensile test. $D_f$ is the failure damage value corresponding to the uniaxial strain $\varepsilon_f$.

### 7.1. Mesh sensitivity for the RTCL criterion

The mesh sensitivity is handled by a mesh scaling curve, given by the following expression

$$D_{\text{cr}}\left(\frac{t}{l_e}, T = 0.33\right) = \varepsilon_f\left(\frac{t}{l_e}\right) = n + (\varepsilon_n - n)\frac{t}{l_e}. \tag{10}$$

This is derived analytically based on virtual local necks appearing within large elements. Here, $n$ is the power law exponent and diffuse necking strain and $\varepsilon_n$ is the failure strain at $t/l = 1$ at uniaxial stress. For the given material these values are equal to $n = 0.205$ and $\varepsilon_n = 0.67$. This is a material specific curve which accounts for the material localization effect only. Strain concentration effects due to geometry such as crack tips and structural arrangement can only be accounted for by mesh refinement.

### 7.2. Implementation of the RTCL criteria

The RTCL model is not a default fracture criterion in LS-DYNA, and has therefore been implemented as a user defined subroutine. The material routine itself follows a semi implicit iteration scheme [18] for an isotropic plane stress J2 material. The material curve is represented by the analytical power law relation. The damage calculation is not coupled to the material model, hence the material model shows no softening effect, which is consistent with the large scale element formulation used herein. Element failure is indicated once all integration points have failed. Failure of each through thickness integration points occurs when the critical damage is violated. At this point the stiffness is set to zero, as to simulate a growing through thickness crack. The mesh effect is automatically taken care of by the material routine, which reads and stores the initial element thicknesses and lengths. The critical damage is then scaled according to the element size.

## 8. Results

Compliance of the material models applied in LS-DYNA was considered comparing the non-failure subjected simulations, shown as an example in Fig. 11 for the 50 mm mesh size. Resulting force–penetration curves for the different mesh sizes and applied failure criteria are given in Fig. 12 for the test section 1, in Fig. 13 for the test section 2 and in Fig. 14 for the test section 3.

Figure 15 compares the reference solution obtained by Peschmann [3] including the experimental clamping arrangement and initial velocity of 2.5 m/s in normal direction and 0.131 m/s in perpendicular direction. The static friction coefficient was 0.3, dynamic friction was neglected. Peschmann used a yield strength of

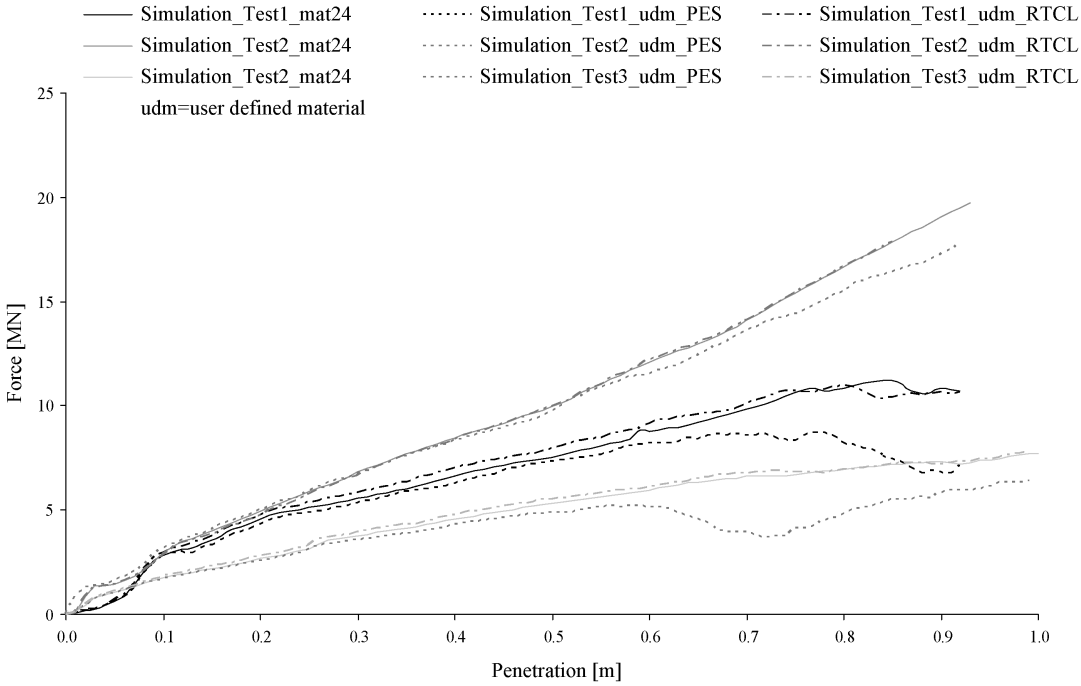


Fig. 11. LS-DYNA material model validation.

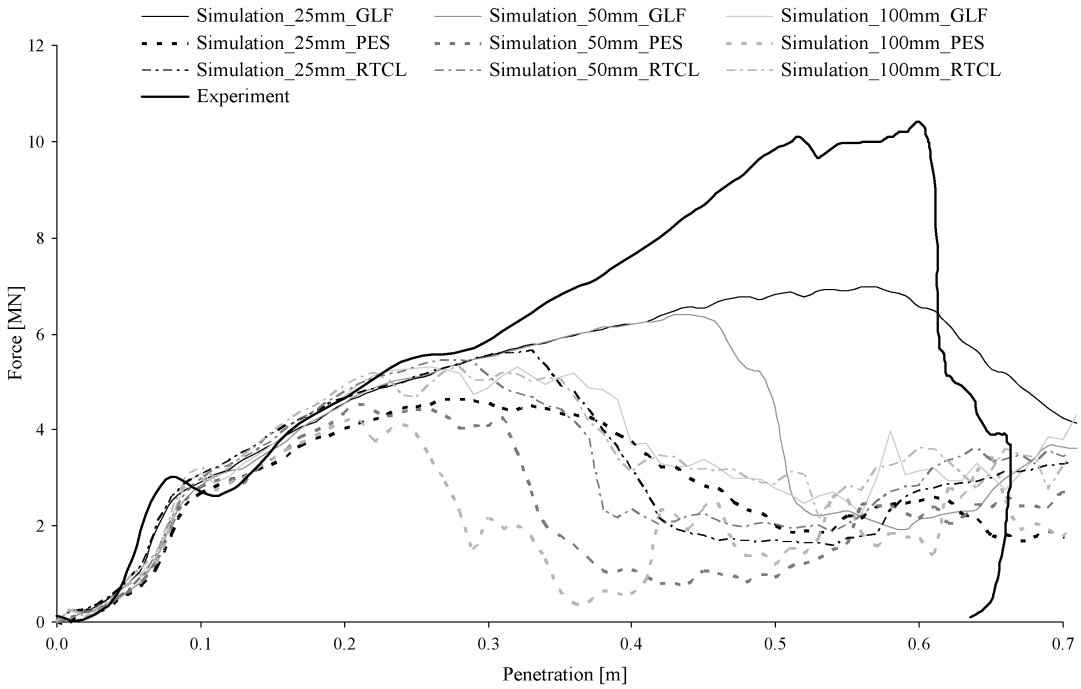


Fig. 12. Test section 1 results and comparison.

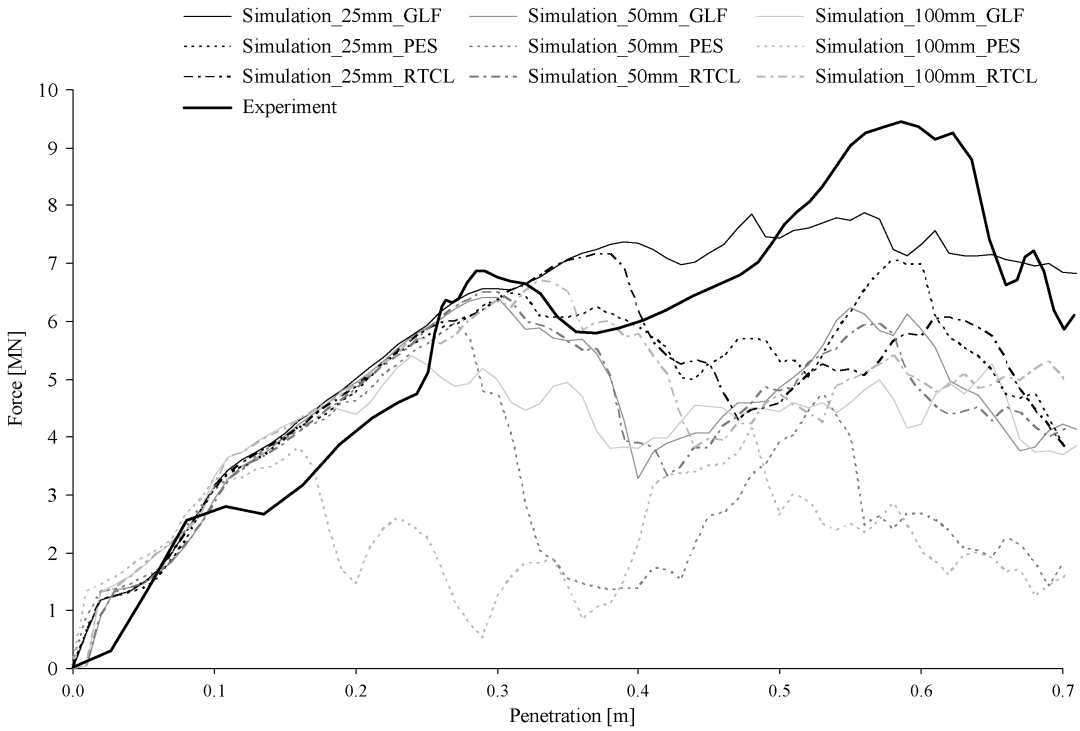


Fig. 13. Test section 2 results and comparison.

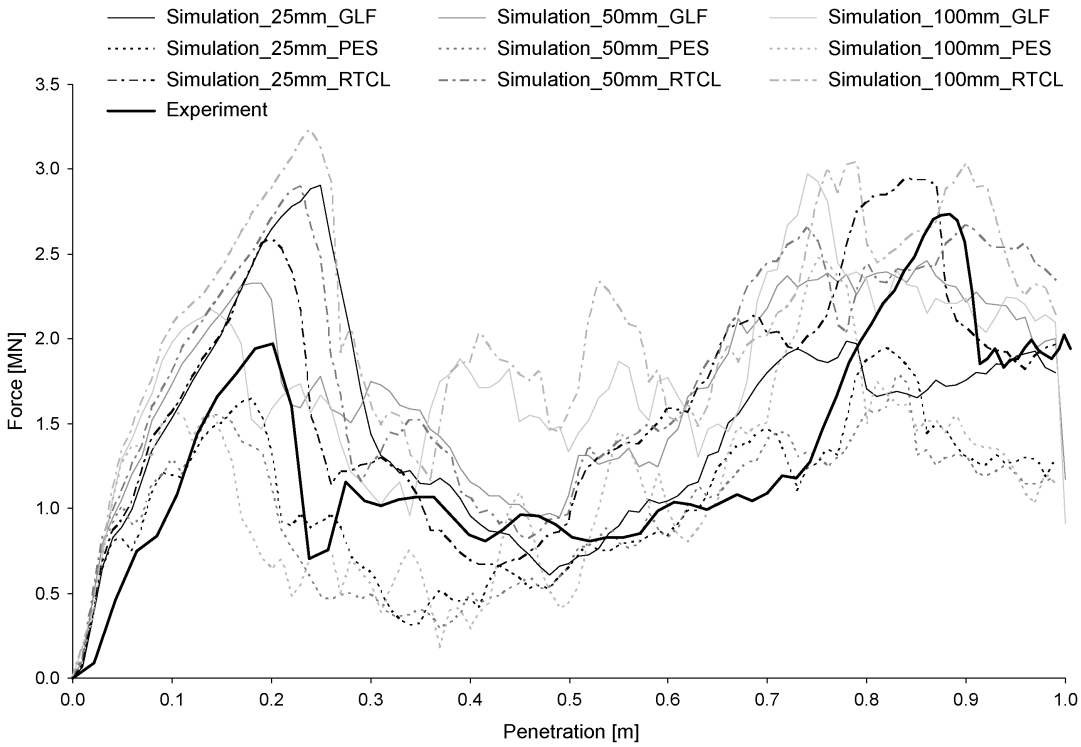


Fig. 14. Test section 3 results and comparison.

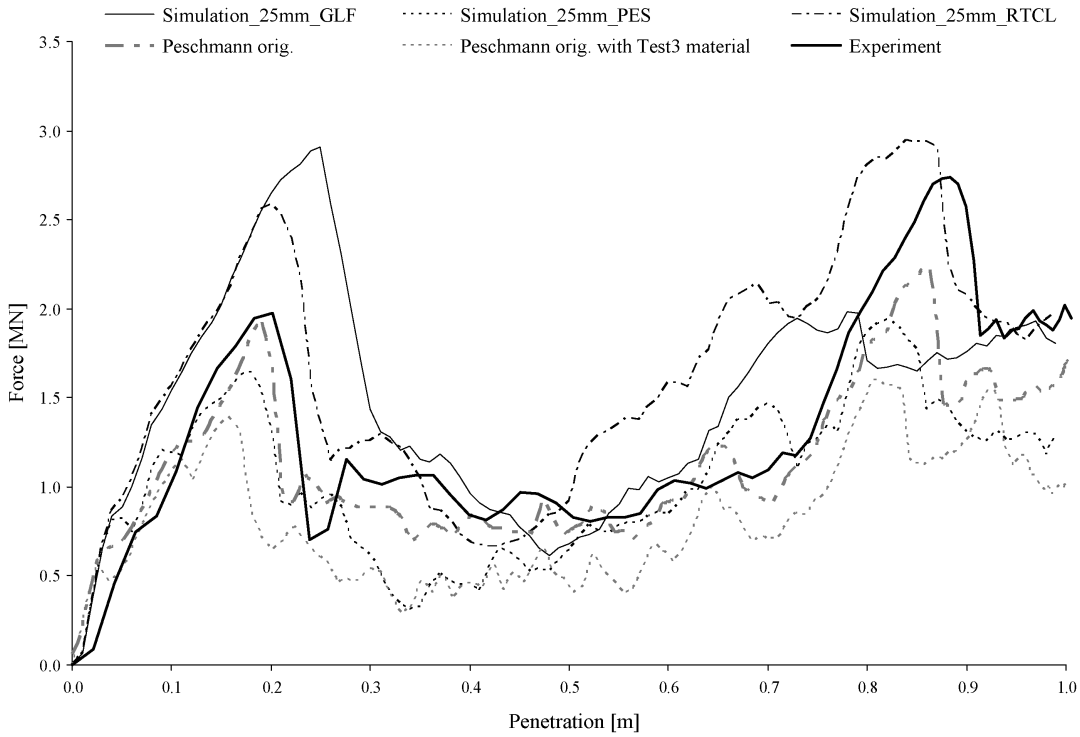


Fig. 15. Test section 3 results including results from Peschmann [3].

312 MPa and a power law with $K = 760$ and $n = 0.187$. In addition to Peschmann's original material data, one solution is included applying the material data according to this benchmark study.

Intermediate penetration stages are presented in Table 1 for a visual evaluation of the failure propagation under the applied failure criteria.

## 9. Discussion

The applied material number 123 from LS-DYNA and the user defined material for the PES and RTCL criteria implemented correlate well for the non failure subjected simulations, see Fig. 11.

The simulations have been performed with a constant indenter velocity of 10 m/s. The experimental curves are obtained with decreasing velocities starting around 4 m/s. When a fully coupled analysis between external dynamics and internal mechanics is of interest the decrease in velocity can be considered. Prescribed velocities, assuming the knowledge of the real velocity histories, will influence the result (see Fig. 15 and [3]) and allow a better comparison to the experiment. Pre-existing experimental results however are unusual in the case of a collision or grounding simulations. The derivations applying true velocities, various friction coefficients and different boundary conditions can be seen in Konter et al. [19]. Konter et al. found

Table 1
Comparative fracture propagation plots of the 25 mm mesh size, view thru the indenter

| Test/Criteria | GLF | PES | RTCL |
|---|---|---|---|
| Test 1 penetration 0.75 m | 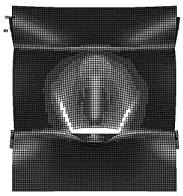 | 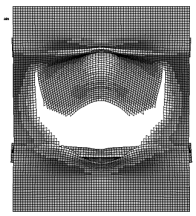 | 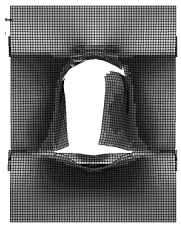 |
| Test 2 penetration 0.75 m | 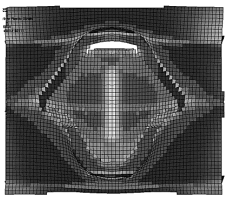 | 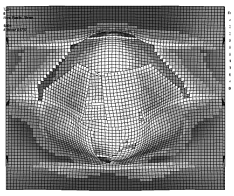 | 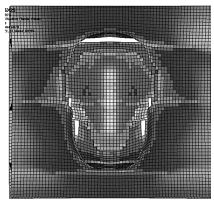 |
| Test 3 penetration 1 m | 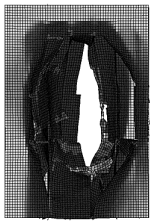 | 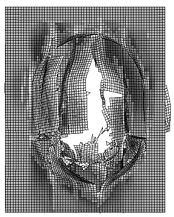 | 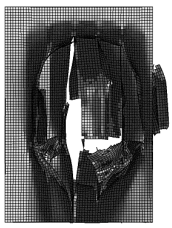 |

no significant effect for the applied velocities or friction coefficients. The colliding speeds are too low for inertia effects to play a role in the calculation, and strain-rate sensitivity is not modeled.

The simulated force–penetration curves of *test section 1* for the applied criteria correspond to the experimental force–penetration curve until rupture is predicted in the simulations, see Fig. 12. The fracture occurs too early when compared to the experiments. The failure criteria and partly the boundary conditions do not capture the membrane deformation mechanism sufficiently. For the GLF criterion the mesh size effect increases with increasing element size. The mesh size sensitivity Eq. (4) seems to be inconsistent. For the PES criterion we see a slight increase in the peak collision force as we decrease the mesh size. The RTCL criterion simulations fracture at about the same penetration distance of 0.35 m. The RTCL load curves follow the other simulations quite well. Fracture initially appears close to the stiffeners, due to the strain concentrations caused by the bulb contact, and the constraint stiffener.

For the simulations of the *test section 2* the GLF criterion captures rupture of the outer plate with the 25 mm mesh with good correspondence to the experimental curve. The 50 mm mesh size, and especially the 100 mm mesh size, do not correspond to experiments. The first peak force value of about 7 MN has not been reached by the PES criterion, failure occurs at 6 MN for the 50 mm mesh size and 6.5 MN for the 25 mm mesh size. The RTCL criterion predicts initial failure quite well for all

meshes, but as soon the tearing process starts, the criterion underpredicts the resistance. The simulations are all on the conservative side. Rupture of the inner plating is not captured sufficiently by any of the mesh sizes and criteria.

*Test section 3* is Peschmann's original test [3]. The simulations of test section 3 shows conservative results for the PES criterion, the GLF and RTCL criterion over predict the experimental force–penetration curve. The 25 mm mesh size of the GLF criterion predicts the inner and outer rupture with a peak value in its force–penetration curve. The coarser meshs do not correspond to the shape of the experimental curve. All criteria show a high degree of mesh sensitivity.

The implementation of the GLF criterion using pre-calculated failure strain values based on the prescribed mesh size can therefore lead to inconsistent results. Prescribing a constant mesh size during the modeling process can result in a various final element sizes, ranging from 80 to 110 mm for a 100 mm mesh, and depending on the geometry. Hence, the predefined failure strain will not be exact according to each element size.

The PES criterion shows a stronger dependency on the plate thickness as covered by Eq. (5). Failure occurs even under pressure, which is physically wrong. The RTCL with its mesh sensitivity criterion, see Eq. (10), handles the various meshes quite well, although, the overall response of the coarsest mesh seem to be a bit too stiff. Even though the RTCL criterion simulations are too optimistic with respect to the strength of the ship side, it does convolute the true results.

For test section 1 the non-failure related curve (see Fig. 11) corresponds very well to the experimental curve until fracture. This clearly indicates that the fracture occurred too early. Possible cause could be that the membrane stretching observed in the test was not captured by the failure criteria. Or the fully clamped boundaries might deviate from the test situation and cause the development of higher strains at an earlier stage leading to premature failure.

The simulation of test section 2 shows a crack initiation between the double side framing and the bulb surface. The inner skin is displaced extra on the cross framing, and for this reason strained to fracture. The fact that fracture seem to occur on the framing membrane intersection for both test section 1 and test section 2 indicates that the stress triaxiality level is quite constant at fracture initiation. Hence, a calibrated effective strain criterion would probably give the same results if calibrated to a stress triaxiality ranging between plane strain and biaxial strain ($T = 0.5667$ and $0.6667$).

The fact that the coarse meshes of test section 3 show a much stiffer response than the finer meshes indicate that there is a high degree of stress and strain concentrations before fracture, which is not captured by the large sized elements. Fracture initiates close to the cross-sectional girder-frame structure, which cannot be covered by a coarse mesh. This is not an effect of local necking within large elements, but an effect due to geometry constraints which causes stress and strain concentration. This can only be accounted for by a mesh refinement.

Peschmann's original test section 3 model included the full clamping system, as well as the prescribed true velocities of the indenter. The comparison presented in

Fig. 15 shows an increase of the force–penetration curve of about 25% owing to the different material model, friction coefficients, velocity decomposition and boundary conditions. With this difference in mind, the PES criterion approximates the experiments fairly good.

The results of the visual failure propagation comparison for the applied criteria show diverse paths, specifically openings in the plating. The latter might be important when oil outflow areas are of interest. However, this part of the simulations requires further research.

## 10. Conclusion

The benchmark study was successfully performed. The results indicate that for coarser meshes the deletion of elements has a greater influence on the force than for the fine mesh. The 100 mm mesh size is too coarse to capture the failure propagation sufficiently for the test sections, however for the GLF and PES criteria the prescribed $l/t > 5$ ratio results in coarse meshes. Improvements could be done by mesh refinements. A common equation to account for the mesh size sensitivity should be used. Handling the mesh size sensitivity might be more important than the criterion itself for the presented cases, as the different results are obtained by different mesh sensitivity equations. A finer mesh in combination with a non local criterion, or a finely meshed solid model to take care of the true stress state in all directions, could correspond better to the experimental results. User defined material models allow the consistent application of failure criteria as the critical strain is computed for each actual element length. Care has to be taken when identifying the actual element length. Averaging the four element sides suffices. To increase the accuracy of the material model, necessary parameters shall be obtained from experiments involving the material applied in the structure to be analyzed.

## Acknowledgments

This study has been supported by the MARSTRUCT network of excellence on ship structures funded by the European commission (http://www.mar.ist.utl.pt/marstruct/; contract: TNE3-CT-2003-506141). This help is here kindly appreciated. Furthermore, the EU STREP DSS_DC program is acknowledged for supporting the work of PhD candidate H. Alsos.

## References

[1] A.E. Mansour and R.C. Ertekin, in: *Proceedings of the 15th International Ship and Offshore Structures Congress*, Vol. 2, Elsevier, 2003, pp. 84–86.

[2] P.A. Frieze and R.A. Shenoi, in: *Proceedings of the 15th International Ship and Offshore Structures Congress*, Vol. 2, 2006, pp. 21–23.

[3] J. Peschmann, Energy absorption computations of ship steel structures under collision and grounding (translated from German language), Doctoral Dissertation, Technical University of Hamburg, 2001.

[4] R. Törnqvist and B.C. Simonsen, Experimental and numerical modeling of ductile crack propagation in large-scale shell structures, *Marine Structures* **17** (2004), 1–27.

[5] R. Törnqvist, Design of crashworthy ship structures, PhD Dissertation, Department of Naval Architecture and Offshore Engineering, Technical University of Denmark, 2003.

[6] O. Kitamura, T. Kuroiwa et al., A study on the improved tanker structure against collision and grounding damage, in: *Proceedings of the Seventh International Symposium on Practical Design of Ships and Mobile Units (PRADS)*, Elsevier Science B.V., The Hague, The Netherlands, 1998, pp. 173–179.

[7] J. Peschmann, A. Kulzep and E. Lehmann, Structural behaviour of double-hull ships in collision and grounding, Ship Technology Research, Shiptechnology, Vol. 49-2002, Hamburg, 2002.

[8] R. Törnqvist, Numerical prediction of ultimate strength, crushing of steel structures, Master Thesis, Department of Naval Architecture and Offshore Engineering, Technical University of Denmark, 2000, p. 108.

[9] H. Alsos, A comparative study in element deletion and element splitting, Master Thesis (ICL report 127), Impact and Crashworthiness Laboratory, Massachusetts Institute of Technology, 2004, pp. 38–39.

[10] LS-Dyna Keyword User's Manual, Livermore Software Technology Corporation, Version 970, 2003, pp. 281–320 and pp. 387–392.

[11] J. Broekhuijsen, Ductile failure and energy absorption of Y-shape test section, Master Thesis, Delft University of Technology, The Netherlands, 2003.

[12] D.W.A. Rees, *Basic Engineering Plasticity, An Introduction with Engineering and Manufacturing Applications*, Elsevier, 2006.

[13] M. Scharrer, L. Zhang and E.D. Egge, Final report MTK0614, Collision calculations in naval design systems, Report Nr. ESS 2002.183, Version 1/2002-11-22, Germanischer Lloyd, Hamburg, 2002.

[14] L. Zhang, E.D. Egge and H. Bruhns, Approval procedure concept for alternative arrangements, in: *Proceedings of the 3rd International Conference on Collision and Grounding of Ships (ICCGS)*, IZU, Japan, 2004, pp. 87–96.

[15] J. Peschmann and A. Kulzep, Final report for BMBF Life-Cycle Design, Part D2A: Side collision of double skin ships, Technical University of Hamburg, 2000 (Contract BMBF 18S0129).

[16] J. Rice and D. Tracey, On the ductile enlargement of voids in triaxial stress fields, *Journal of the Mechanics and Physics of Solids* **17** (1969), 201–217.

[17] M.G. Crockcroft and D.J. Latham, Ductility and the workability of metals, *J. Inst. Metals* **96** (1968), 33–39.

[18] T. Belytschko, W.K. Liu and B. Moran, *Nonliniar Finite Elements for Continua and Structures*, John Wiley & Sons Ltd., 2000.

[19] A. Konter, J. Broekhuijsen and A. Vredeveldt, A quantitative assessment of the factors contributing to the accuracy of ship collision predictions with the finite element method, in: *Proceedings of the 3rd International Conference on Collision and Grounding of Ships (ICCGS)*, IZU, Japan, 2004, pp. 17–26.